

# Inferring Multi-Dimensional Rates of Aging from Cross-Sectional Data

Emma Pierson<sup>\*12</sup> Pang Wei Koh<sup>\*12</sup> Tatsunori Hashimoto<sup>\*1</sup>  
Daphne Koller<sup>23</sup> Jure Leskovec<sup>1</sup> Nicholas Eriksson<sup>24</sup> Percy Liang<sup>1</sup>

## Abstract

Modeling how individuals evolve over time is a fundamental problem in the natural and social sciences. However, existing datasets are often *cross-sectional* with each individual only observed at a single timepoint, making inference of temporal dynamics hard. Motivated by the study of human aging, we present a model that can learn temporal dynamics from cross-sectional data. Our model represents each individual with a low-dimensional latent state that consists of 1) a dynamic vector  $rt$  that evolves linearly with time  $t$ , where  $r$  is an individual-specific “rate of aging” vector, and 2) a static vector  $b$  that captures time-independent variation. Observed features are a non-linear function of  $rt$  and  $b$ . We prove that constraining the mapping between  $rt$  and a subset of the observed features to be *order-isomorphic* yields a model class that is identifiable if the distribution of time-independent variation is known. Our model correctly recovers the latent rate vector  $r$  in realistic synthetic data. Applied to the UK Biobank human health dataset, our model accurately reconstructs the observed data while learning interpretable rates of aging  $r$  that are positively associated with diseases, mortality, and aging risk factors.

## 1. Introduction

Understanding how individuals evolve over time is an important problem in fields such as aging (Belsky et al., 2015), developmental biology (Waddington, 1940), cancer biology (Nowell, 1976), ecology (Jonsen et al., 2005), and economics (Ram, 1986). However, observing large-scale temporal measurements of individuals is expensive and sometimes

even impossible due to destructive measurements (e.g., in sequencing-based assays (Campbell & Yau, 2017)). As a result, we often only have *cross-sectional data*—each individual is only measured at one point in time (though different individuals can be measured at different points in time). From this data, we wish to learn *longitudinal models* that allow us to make inferences about how individuals change over time.

This work was motivated by the problem of studying human aging using data from the UK Biobank, which contains extensive health data for half a million participants of ages 40–70 (Sudlow et al., 2015). The UK Biobank is unique among health datasets in the breadth and sheer scale of its data. However, most of its data is cross-sectional; 95% of its participants are measured at a single time point.

Can we learn temporal dynamics purely from cross-sectional data? While impossible in general (Hashimoto et al., 2016), this inference has been carried out in restricted settings. For example, single-cell RNA-seq studies use pseudotime methods to reconstruct temporal trajectories from cross-sectional data (Campbell & Yau, 2017; Trapnell et al., 2014; Bendall et al., 2014). These methods typically assume that individuals start at the same location and travel along the same single-dimensional trajectory (up to a few branching points). These assumptions are not realistic for studying human aging, which is a multi-dimensional process (McClean, 1997): for example, someone might stay relatively physically fit but experience cognitive decline or vice versa (Figure 1). Moreover, there is substantial aging-independent variation across individuals (e.g., intrinsic differences in height).

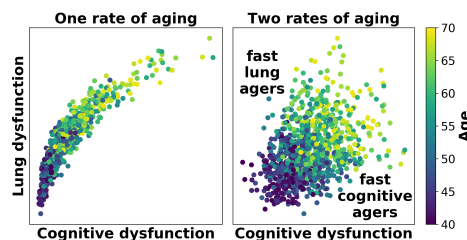


Figure 1. Toy example. Multiple rates of aging (right) allow for some individuals to progress rapidly in one aging dimension, and others to progress rapidly in another.

<sup>\*</sup>Equal contribution <sup>1</sup>Department of Computer Science, Stanford University, USA <sup>2</sup>Calico Life Sciences LLC, South San Francisco, USA <sup>3</sup>Now at Insitro, Inc. <sup>4</sup>Now at 23andMe, Inc. Correspondence to: Emma Pierson <emmap1@cs.stanford.edu>, Pang Wei Koh <pangwei@cs.stanford.edu>.

In this paper, we introduce a generative model that can learn such a multi-dimensional temporal process from cross-sectional data. We represent each individual with a low-dimensional latent state comprising a dynamic vector  $rt$  that evolves linearly with time  $t$  (with the rate of evolution specified by an individual-specific rate vector  $r$ ) and a static bias vector  $b$  that encodes time-independent variation. An individual’s observations are modeled as a non-linear function of their latent state  $rt$  and  $b$ . In the aging context,  $r$  captures the age-dependent progression of different groups of phenotypes (e.g., muscle strength vs. cognitive ability), while  $b$  factors out age-independent individual variation.

We first study the question of identifiability: under what conditions is it possible to learn the above model from the cross-sectional data that it generates? The key structure that we leverage to make our model identifiable is the *monotonicity* of the mapping between the time-evolving state  $rt$  and a subset of the observed features. This captures the intuition that aging is a gradual process where many systems show a generally-monotone decline after the age of 40 (e.g., weight (Mozaffarian et al., 2011), red blood cell measurements (Hoffmann et al., 2015), lung function (Stanojevic et al., 2008), and lean muscle mass (Goodpaster et al., 2006)). We prove that if the distribution of time-independent variation is known, monotonicity gives us identifiability of the model. Our work strengthens the earlier work of Hashimoto et al. (2016), which showed identifiability for general diffusion processes, but only in the noiseless setting and with an infinite number of observed timepoints.

We learn this monotone generative model with a variational autoencoder (Kingma & Welling, 2014), constraining the decoder mapping from  $rt$  to a subset of the observed features to be monotone. We further show how to extend our learning procedure to incorporate any longitudinal data that has been collected.

We assess our model using data from the UK Biobank cohort: specifically, 52 phenotypes measured for more than 250,000 individuals aged 40-70. Our model learns an interpretable, low-dimensional representation of how human phenotypes change with age, accurately reconstructing the observed data and predicting age-related changes in each phenotype. Through posterior inference on the rate vector  $r$ —which we can interpret as a rate of aging— we recover several dimensions of aging, each corresponding to one coordinate of  $r$ , which have natural interpretations relating to changes in different body systems (e.g., cognitive performance and lung health). Higher inferred rates of aging are associated with disease, mortality, and known risk factors (e.g., smoking). These rates can be used in downstream applications, such as genome-wide association studies, to identify genetic variants that affect the rates at which an individual ages.

## 2. Model

Let  $x_t \in \mathbb{R}^d$  be the observed features of an individual at time  $t$ . A classic approach to modeling temporal progression is to assume that  $x_t$  depends linearly on some latent measure of progression  $z_t \in \mathbb{R}$  plus Gaussian noise. Examples include Klemra & Doubal (2006) and Levine (2012) in the context of human aging—where  $z_t$  is often called *biological age*— and Campbell & Yau (2017) in the context of gene expression. We extend this approach in three ways: we allow  $x_t$  to depend non-linearly on  $z_t$  and a bias term; we constrain some components of  $x_t$  to depend monotonically on  $z_t$ ; and we allow  $z_t$  to have multiple dimensions.

Specifically, we characterize each individual by two latent variables:

1. A *rate* vector  $r \in \mathbb{R}^{k_r}$  that determines how rapidly an individual is changing over time, and
2. A *bias* vector  $b \in \mathbb{R}^{k_b}$  that encodes time-independent variation.

$r$  and  $b$  are fixed for each individual and do not change over time. For interpretability, we model each individual as evolving linearly in latent space at a rate proportional to  $r$ , i.e.,  $z_t = rt$ , and we model  $x_t$  as the sum of a time-dependent component  $f(rt)$  and time-independent component  $g(b)$ :

$$x_t = f(rt) + g(b) + \epsilon. \quad (1)$$

Here,  $f: \mathbb{R}^{k_r} \rightarrow \mathbb{R}^d$  is a non-linear function capturing time-dependent variation;  $g: \mathbb{R}^{k_b} \rightarrow \mathbb{R}^d$  is a non-linear function capturing time-independent variation; and  $\epsilon$  is measurement noise sampled i.i.d. at each time point. We assume that  $r$ ,  $b$ , and  $\epsilon$  are independently drawn from known priors, and that the rates  $r$  are always positive (so that there is no “reverse aging”).

**Monotonicity.** To ensure that the model is identifiable from cross-sectional data, we make the structural assumption that some coordinates of  $f$  are *monotone*. Roughly speaking, this means that as  $t$  increases, those coordinates of  $f(rt)$  will also increase on average; we defer a precise definition to Section 3. The monotonicity of  $f$  is a reasonable assumption in the setting of human aging, as many phenotypes vary monotonically with age after the age of 40 (Mozaffarian et al., 2011; Hoffmann et al., 2015; Stanojevic et al., 2008; Goodpaster et al., 2006). Monotonicity does not imply that, for example, an individual’s strength has to strictly decrease with age (due to  $\epsilon$ ) or that an older individual is always weaker than a younger one (because  $g$  allows for age-independent variation between people).

For identifiability, we will also require  $f^{-1}$  to exist and be monotone in the same phenotypes as  $f$  (Section 3). This

corresponds to the following assumption: if one individual appears older in all phenotypes than another individual, then the former also has an older “biological age” (i.e., larger latent state  $rt$ ) than the latter.

Only  $k_r$  coordinates of  $f$  (corresponding to  $k_r$  phenotypes) need to be monotone for identifiability to hold. To keep notation in the sequel simple, we define  $f$  as monotone and have all non-monotone phenotypes modeled by some other unconstrained  $\tilde{f}$ , i.e.,  $x_t = [f(rt); \tilde{f}(rt)] + g(b) + \epsilon$ . Implicit in this formulation is that the monotone phenotypes are known, so without loss of generality, we order the monotone phenotypes to come before the non-monotone phenotypes.

**Learning.** Our goal is to estimate  $f$ ,  $\tilde{f}$ ,  $g$ , and  $\epsilon$  from cross-sectional data  $\{(t^{(i)}, x_{t^{(i)}}^{(i)})\}_{i=1}^n$ . We parameterize the functions with neural networks and use a variational autoencoder to optimize a standard lower bound on the likelihood of the observed data (Kingma & Welling, 2014); see Section 5 for more details.

### 3. Identifiability

We first study the basic question of identifiability: is it possible to recover  $f$  (and thereby estimate temporal dynamics and rates of aging  $r$ ) from cross-sectional data that is generated by  $f$ ? In other words, do different  $f$  give rise to different observed data?

Without loss of generality, we make three simplifications to the model for our analysis. First, we only consider features  $x$  that correspond to the monotone  $f$ , and disregard the other part which corresponds to  $\tilde{f}$ ; if the model is well-specified and can be identified just by considering  $f$ , then it will remain identifiable when additionally considering the non-monotone part  $\tilde{f}$ . Second, we consider the identifiability of the function  $f$ , rather than parametrizations of the function, since we are not interested in the exact parametrization of  $f$  (e.g., identical functions result in identical posterior estimates for the rates of aging). Third, we consider a single noise term  $\epsilon' \stackrel{\text{def}}{=} g(b) + \epsilon$  which combines age independent variation  $g(b)$  and the measurement noise  $\epsilon$ , since this does not affect the rate of aging.

Together, these give the simplified model

$$x_t = f(rt) + \epsilon'. \quad (2)$$

If  $f$  is a general differentiable function without any monotonicity constraints, there exist functions that are unidentifiable from observations of the distribution of  $x_t$ . As a counterexample, consider  $\epsilon' = 0$  and  $r \sim \text{lognormal}(0, 1)$ . Let  $M$  be any matrix that preserves the all-ones vector  $\mathbf{1}$  and is an orthogonal transform on the orthogonal subspace to  $\mathbf{1}$ . Since  $\log(rt) \sim \mathcal{N}(\log t \mathbf{1}, 1)$ ,  $M \log(rt) \stackrel{(d)}{=}$

$\log(rt)$  due to the rotational invariance of the Gaussian (where  $\stackrel{(d)}{=}$  means equality in distribution). This implies that  $f(\exp(M \log(rt))) \stackrel{(d)}{=} f(rt) \stackrel{(d)}{=} x_t$ . Since  $f(\exp(M \log(\cdot)))$  and  $f(\cdot)$  have the same observed distribution, they are unidentifiable from each other.

This counterexample shows that we need to make additional assumptions on  $f$  to ensure identifiability. Here, we will show that  $f$  is identifiable up to permutation when  $\epsilon'$  is known and both  $f$  and  $f^{-1}$  are monotone—that is,  $f$  is an *order isomorphism*.

**Definition 1.** A function  $f$  is monotone if  $u \preceq v \implies f(u) \preceq f(v)$  for all  $u, v \in \text{dom}(f)$ , where ordering is taken with respect to the positive orthant (i.e.,  $u \preceq v$  means  $u_i \leq v_i$  for all  $i$ ).

**Definition 2.** An injective function  $f$  is an order isomorphism if  $f$  and  $f^{-1}$  restricted to the image of  $f$  are both monotone, that is,  $u \preceq v \iff f(u) \preceq f(v)$ .<sup>1</sup>

#### 3.1. Noiseless setting ( $\epsilon' = 0$ )

We begin by considering the case where  $\epsilon' = 0$ . Our main identifiability result is the following:

**Proposition 1.** Let  $x_t$  and  $rt$  be the random variables defined in (2). If  $f_1$  and  $f_2$  and their inverses are twice continuously differentiable and are order-isomorphic functions such that  $f_1(rt) \stackrel{(d)}{=} f_2(rt) \stackrel{(d)}{=} x_t$  for some  $t > 0$ , then  $f_1$  and  $f_2$  are identical up to a permutation.<sup>2</sup>

We defer proofs to Appendix A. As a proof sketch, we first characterize order isomorphisms:

**Lemma 1.** If  $q: \mathbb{R}^{k_r} \rightarrow \mathbb{R}^{k_r}$  is twice continuously differentiable and an order isomorphism,  $q$  must be expressible as a permutation followed by a component-wise monotone transform.

We then consider the difference map  $q \stackrel{\text{def}}{=} f_2^{-1} \circ f_1$ , which maps the latent state implied by  $f_1$  to that of  $f_2$ .  $q$  is also an order isomorphism, so by Lemma 1 it is the composition of a permutation and monotone map. Since  $f_1(rt) \stackrel{(d)}{=} f_2(rt) \stackrel{(d)}{=} x_t$ ,  $q$  is measure preserving for  $rt$ . As the only monotone measure preserving map is the identity,  $q$  must be a permutation.

#### 3.2. Noisy setting ( $\epsilon' \neq 0$ )

Identifiability in the noisy setting is more challenging. If the noise distribution  $\epsilon'$  is known, we can reduce the question

<sup>1</sup>We deviate from standard nomenclature, where order-isomorphic  $f$  are defined as bijections, by letting  $f$  be injective and considering the restriction of  $f$  to its image.

<sup>2</sup>We define  $f_1$  and  $f_2$  as identical up to permutation if there exists a permutation matrix  $P$  such that  $f_1(Pv) = f_2(v)$ .

of identifiability to that of the noiseless case by first taking the observed distribution of  $x_t$ , deconvolving  $\epsilon'$  gives us the distribution of  $f(x_t)$  from which we can apply Proposition 1. The uniqueness of this procedure follows from the uniqueness of Fourier transforms and inverses over  $L^1$  functions (Stein & Shakarchi, 2011). This corresponds to the setting where we can characterize the distribution of the time-independent variation  $g(b)$  and the measurement noise  $\epsilon$ , either through prior knowledge or measurement (e.g., in a controlled setting where we observe the starting point of all individuals). Importantly, we do not need to know the exact instantiation of  $b$  and  $\epsilon$  for any individual.

If the noise distribution  $\epsilon'$  is unknown, then the characterization we provide here no longer holds, and we cannot simply deconvolve the noise. Nevertheless, we conjecture that the strong structure induced by monotonicity is sufficient for identifiability, and in simulations we are able to recover known ground-truth parameters (Section 6).

#### 4. Learning order isomorphisms

Our identifiability results suggest that we should optimize for  $f$  within the class of order isomorphisms. However, that optimization is difficult in practice, as it requires reasoning about  $f^{-1}$  over the image of  $f$ . Instead, we take the following approach:

1. We relax the order isomorphism constraint and optimize for  $f$  within a class of monotone transformations  $\mathcal{M}$  that have a particular parametrization.
2. We check, post-hoc, if the learned  $f \in \mathcal{M}$  is approximately order-isomorphic. (In real-world optimization settings,  $f$  will not be exactly order-isomorphic for reasons we discuss below.) While not all functions in  $\mathcal{M}$  are order-isomorphic, we choose  $\mathcal{M}$  such that we can quickly verify if a given  $f \in \mathcal{M}$  is approximately order-isomorphic.

While we do not have any prior expectation that the learned  $f$  would be order-isomorphic, surprisingly, we find in our experiments (Section 5) that we do in fact learn an approximately order-isomorphic  $f \in \mathcal{M}$ . In our experiments, at least, constraining  $f$  to be monotone gives us approximate order isomorphism for free. This suggests that we do not lose any representational power by moving from monotone functions to order-isomorphic functions, and that the assumption of order isomorphism (on top on monotonicity) is reasonable here.

We choose  $\mathcal{M}$  to be the set of functions that can be written as  $f: \mathbb{R}^k \rightarrow \mathbb{R}^d = s_2 \circ a \circ s_1$ , where  $s_1: \mathbb{R}^k \rightarrow \mathbb{R}^k$  and  $s_2: \mathbb{R}^d \rightarrow \mathbb{R}^d$  are continuous, component-wise monotone

transformations,<sup>3</sup> and  $a: \mathbb{R}^k \rightarrow \mathbb{R}^d$  is a linear transform. Note that all  $f \in \mathcal{M}$  are monotone by construction, due to the compositionality of monotone functions.

The following results show that we can check if some  $f \in \mathcal{M}$  is order-isomorphic, i.e.,  $f^{-1}$  is also monotone, by examining only the linear transform  $a$ :

**Lemma 2.** *Let  $a(v) = Av$  be a linear transform, where  $A \in \mathbb{R}^{d \times k}$ . If we can write  $A = P \begin{bmatrix} B \\ C \end{bmatrix}$  where  $P$  is a permutation matrix,  $B$  is a non-negative monomial matrix,<sup>4</sup> and  $C$  is a non-negative matrix, then  $a$  is an order isomorphism.*

**Proposition 2.** *Let  $f: \mathbb{R}^k \rightarrow \mathbb{R}^d = s_2 \circ a \circ s_1$ , where  $s_1: \mathbb{R}^k \rightarrow \mathbb{R}^k$  and  $s_2: \mathbb{R}^d \rightarrow \mathbb{R}^d$  are continuous, component-wise monotone transformations, and  $a: \mathbb{R}^k \rightarrow \mathbb{R}^d$  is a linear transform. If  $a$  satisfies Lemma 2, then  $f$  is an order isomorphism.*

We defer proofs to Appendix A.5.

Correspondingly, during training, we restrict  $f$  to the form  $s_2 \circ a \circ s_1$ , where  $s_1$  and  $s_2$  are component-wise monotone transforms and  $a$  is a linear transformation parameterized by  $A$ , a non-negative matrix. This function can be optimized straightforwardly: we parametrize  $s_1$  and  $s_2$  as polynomials with non-negative coefficients and do gradient descent on the coefficients, though this can be swapped out with other differentiable parameterizations of monotone functions (Gupta et al., 2016).

To check if  $f$  is order-isomorphic, Proposition 2 tells us that  $a$  needs to satisfy the conditions of Lemma 2. This is equivalent to checking if every column of  $A$  has a non-zero element in a row where every other column has a zero. In our fitted model, we find that the learned  $A$  is close to this structure, although the learned entries of  $A$  are only approximately, not exactly, 0. To verify that  $A$  contained a matrix that was essentially monomial, we confirmed that each column  $j$  contained at least one row  $i$  where  $A_{ij} \gg A_{ik}, k \neq j$ ; specifically,  $A_{ij} > 50A_{ik}$ .<sup>5</sup> Thus, by learning a monotone  $f$ , we also learn an approximately monotone  $f^{-1}$  without any further constraints.

<sup>3</sup> $s$  is a component-wise transformation if it acts separately on each component of its input, i.e.,  $s(v) = [s_1(v_1), s_2(v_2), \dots, s_k(v_k)]$ .

<sup>4</sup>A monomial matrix is a square matrix in which each row and each column has only one non-zero element. In other words, it is like a permutation matrix, except that the non-zero elements can be arbitrary.

<sup>5</sup>In our experiments (Section 5), we find that using only a single monotone component-wise transform ( $f = s_2 \circ a$ ) does not significantly harm performance, and so use only a single component-wise transform  $s_2$  for interpretability. This means that the relative magnitudes of  $A_{ij}$  and  $A_{ik}$  are meaningful because the columns of  $A$  are not arbitrarily scaled by the component-wise transform.

## 5. Experimental setup

**Data processing.** We describe the full dataset processing procedure in Appendix B. In brief, we selected features that were measured for most participants, resulting in 52 phenotypes across the following categories: spirometry (a measure of lung function), bone density, body type/anthropometry, cognitive function, vital signs (blood pressure and heart rate), physical activity, hand grip strength, and blood test results. By visual inspection, we categorized these 52 phenotypes into monotone (45/52) and non-monotone features (7/52). For convenience, we pre-processed the monotone phenotypes to all be monotone increasing with age by negating them if necessary. After filtering, we were left with a train/development set of 213,510 individuals with measurements at a single time point; we report all results on a separate test set of 53,174 individuals not used in model development or selection. We also have longitudinal data from a single followup visit for an additional 8,470 individuals.

**Model details.** We use a variational autoencoder to learn and perform inference in our model (Kingma & Welling, 2014). We parameterize the monotone function  $f = s \circ a$  as the composition of a monotone elementwise transformation  $s: \mathbb{R}^{d'} \rightarrow \mathbb{R}^{d'}$  with a monotone linear transform  $a: \mathbb{R}^{k_r} \rightarrow \mathbb{R}^{d'}$ .<sup>6</sup>

We parameterize the linear transformation  $a$  using a matrix  $A$  constrained to have non-negative entries, and implement each component  $s_i(v): \mathbb{R}_+ \rightarrow \mathbb{R}_+$  of  $s$  as the sum of positive powers of  $v \in \mathbb{R}_+$  with non-negative coefficients  $s_i(v) = \sum_{p_j \in S} w_{ij} v^{p_{ij}}$ , where  $w_{ij}$  are learned non-negative weights, and  $S$  is a hyperparameter. (For example,  $S = [\frac{1}{2}, 1, 2]$  yields the function class  $s(v) = w_0 v^{\frac{1}{2}} + w_1 v + w_2 v^2$ .) We verified that the learned model’s  $A$  matrix (part of the monotone function  $f$ ) can be row-permuted into a combination of an approximately monomial matrix and positive matrix, indicating that we learned an  $f$  that was order-isomorphic (Section 4).

We use neural networks to parameterize the non-monotone functions  $\tilde{f}$  and  $g$  as well as the encoder (which approximates the posterior over the latent variables  $r$  and  $b$ ). We adopt the following priors:  $r \sim \text{lognormal}(0, \sigma_r^2 I)$ ;  $b \sim \mathcal{N}(0, I)$ ; and  $\epsilon \sim \mathcal{N}(0, \sigma_\epsilon^2 I)$ . We use a lognormal distribution for  $r$  to ensure positivity; set  $\sigma_r = 0.1$  to reflect a realistic distribution of the rates of biological aging (Belsky et al., 2015); and optimize over  $\sigma_\epsilon$ . Finally, we simply take  $t$  to be an individual’s age, although we could also have optimized over some constant  $t_0$  and taken  $t = \text{age} - t_0$ .

<sup>6</sup> We explored using two monotone elementwise transformations  $s_1$  and  $s_2$ , but found that removing the second transformation did not greatly affect performance, and so used the simpler model class for interpretability.

### Hyperparameter search and latent state size selection.

We selected all hyperparameters other than the size of the latent states  $k_r$  and  $k_b$  (e.g., network architecture and the set of polynomials  $S$ ) through random search evaluated on a development set (Appendix C). Increasing  $k_r$  and  $k_b$  gives the model more representational power; indeed, test ELBO increased uniformly with increasing  $k_b$  and  $k_r$  in the range we tested ( $k_b + k_r \leq 20$ , to force the model to learn a compressed representation of the 52 phenotypes). We chose  $k_b = 10$  and  $k_r = 5$  to balance modeling accuracy with dimensionality reduction for interpretability, since the test ELBO begins to level off at  $k_r = 5$ ; we chose a higher  $k_b$  since we are not as concerned with dimensionality reduction for the time-independent variation. Our results were qualitatively similar with other values of  $k_r$  and over multiple random seeds.

## 6. Results on synthetic data

We evaluated whether we could correctly recover the rates of aging  $r$  in the well-specified setting (where the data is generated by the model with some ground truth value of  $r$ ). As  $r$  is a latent quantity, we had to assess this on synthetic data to get ground truth. To generate realistic synthetic data, we fit the model described in Section 5 to data from the UK Biobank and then sampled from it. We verified that this synthetic data matched the properties of UK Biobank data, e.g., the sampled age trends for each feature were close to the age trends of the observed data; we describe this in more detail in Section 7.

We then fit a second model with the same model structure to the synthetic data and checked if the posterior means of the rates of aging  $r_{\text{fitted}}$  inferred by the second model matched those inferred by the true generative model,  $r_{\text{true}}$  (up to permutation). We ran this check for models with different values of  $k_r = 1, 2, \dots, 10$  and found good concordance across all values of  $k_r$ : the mean correlation between  $r_{\text{fitted}}$  and  $r_{\text{true}}$  was 0.91, and the slopes of the regressions of  $r_{\text{fitted}}$  on  $r_{\text{true}}$  were very close to one (mean absolute difference from 1 of 0.09), indicating good calibration.

## 7. Results on UK Biobank data

### 7.1. Accuracy in reconstruction and extrapolation

We first show that our model can *reconstruct* each datapoint from its low-dimensional projection and can *extrapolate* to future timepoints, predicting what individuals will look like in the future. The goal of these evaluations is not to demonstrate state-of-the-art predictive performance; rather, we want to verify that our model accurately reconstructs individual datapoints and captures aging trends. After sanity checking that the model accurately captures these features of the distribution, we assess the interpretability of the learned

rates of aging in Section 7.2 below.

**Reconstruction.** We assessed if our model was able to reconstruct observed datapoints from their latent space projections without a significant loss in accuracy. Given an observation  $(t, x_t)$ , we computed the approximate posterior mean of the latent variables  $(\hat{r}, \hat{b})$  using the encoder, and compared  $x_t$  against the reconstructed posterior mean of  $x_t$  given  $(\hat{r}, \hat{b})$ . On a held-out test set, we found reconstruction to be largely accurate: the mean correlation between true and reconstructed feature values was 0.88, and the mean squared reconstruction loss was 0.23 on a scale where each feature has variance 1.

As a simple baseline, principal components analysis (PCA) with the same number of latent states ( $k_r + k_b = 15$ ) performed comparably but slightly worse, achieving a mean correlation of 0.86 and a mean squared reconstruction loss of 0.25.<sup>7</sup> We compare with PCA because it is commonly used in biological studies (Relethford et al., 1978); although PCA is a linear model, it optimizes explicitly for reconstruction error and does not need to account for any priors on latent variables. This demonstrates that our model, in spite of its monotonic constraints and priors on the latent variables, reconstructs the observed data at least as accurately as a widely used reconstruction baseline, while additionally providing (as we discuss below) an interpretable latent state.

**Extrapolation to future timepoints.** To assess how accurately the model captures the aging process, we evaluate its ability to “fast-forward” people through time: that is, to predict their phenotype  $x_{t_1}$  at a future age  $t_1$  given their current age  $t_0$  and phenotype  $x_{t_0}$ . As above, we compute the posterior means  $(\hat{r}, \hat{b})$  using  $x_{t_0}$  and  $t_0$ ; we then predict  $x_{t_1} = f(t_1, \hat{r}) + g(\hat{b})$ .

We assess the accuracy of fast-forwarding on both cross-sectional and longitudinal data. On cross-sectional data, we do not have follow-up data  $x_{t_1}$  for each person, so we evaluate the model by *age group*: for example, we fast-forward all 40–45 year olds by 5 years, compute how much the model predicts each feature will change on average, and compare that to the true average feature change between 40–45 year olds and 45–50 year olds. (Although we bucket age in this analysis to reduce noise, the model uses the person’s exact age.) Predictions are highly correlated with the true values ( $r = 0.77$  for 5-year followups, Figure 2;  $r = 0.88$  for 10 years, and 0.94 for 15 years).

On longitudinal data, we observe both  $x_{t_0}$  and  $x_{t_1}$  for a single person, and can therefore use reconstruction accuracy of  $x_{t_1}$  as a metric. This is a difficult task because longi-

<sup>7</sup>We evaluate PCA reconstruction loss both when PCA is provided age as an input, and when it is not; its reconstruction loss is virtually identical regardless.

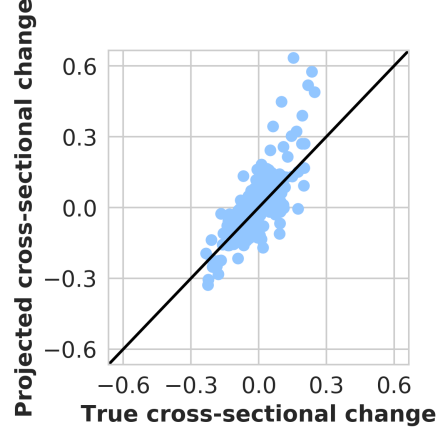


Figure 2. True and predicted changes in each feature are well-correlated ( $r = 0.77$ ) in cross-sectional data when fast-forwarding 5 years. Each point represents the difference in one feature for one 5-year age bin: e.g., the difference in systolic blood pressure between 40–45 and 45–50 year olds.

tudinal follow-up times are very short in our dataset (2–6 years), so aging-related changes may be swamped by the inherent noise in the task; further, the model is not fitted on the longitudinal data, which may have different biases than the cross-sectional data. To evaluate model performance, we compare to three baseline methods, and compute the fraction of people for which our model yields lower reconstruction error; we use this metric rather than the average error because the noise in the data is large relative to aging-related change, so the average improvement for a particular individual will be small even if one method consistently yields better predictions for the whole population. For follow-up times long enough to allow for substantial age-related change ( $> 5$  years), our model predicts  $x_{t_1}$  more accurately than all three baselines: just predicting  $x_{t_0}$  (which incurs higher error on 66% of people); just reconstructing  $x_{t_0}$  without fast-forwarding (higher error on 61%); or fast-forwarding each person by assuming that each of their features changes by the average rate of change in cross-sectional data (higher error on 60%). We show how to further improve these results in Section 7.3 below.

## 7.2. Model interpretation

Next, we interpreted the learned dimensions of aging and evaluated if they matched up with known biology. Empirically, we found that enforcing monotonicity in  $f$  encouraged sparsity, producing interpretable rates of aging: we simply associated each rate of aging with the sparse set of features that it was correlated with. (If we did not enforce monotonicity, the rates of aging would not be associated with sparse sets of features, rendering them less interpretable.)



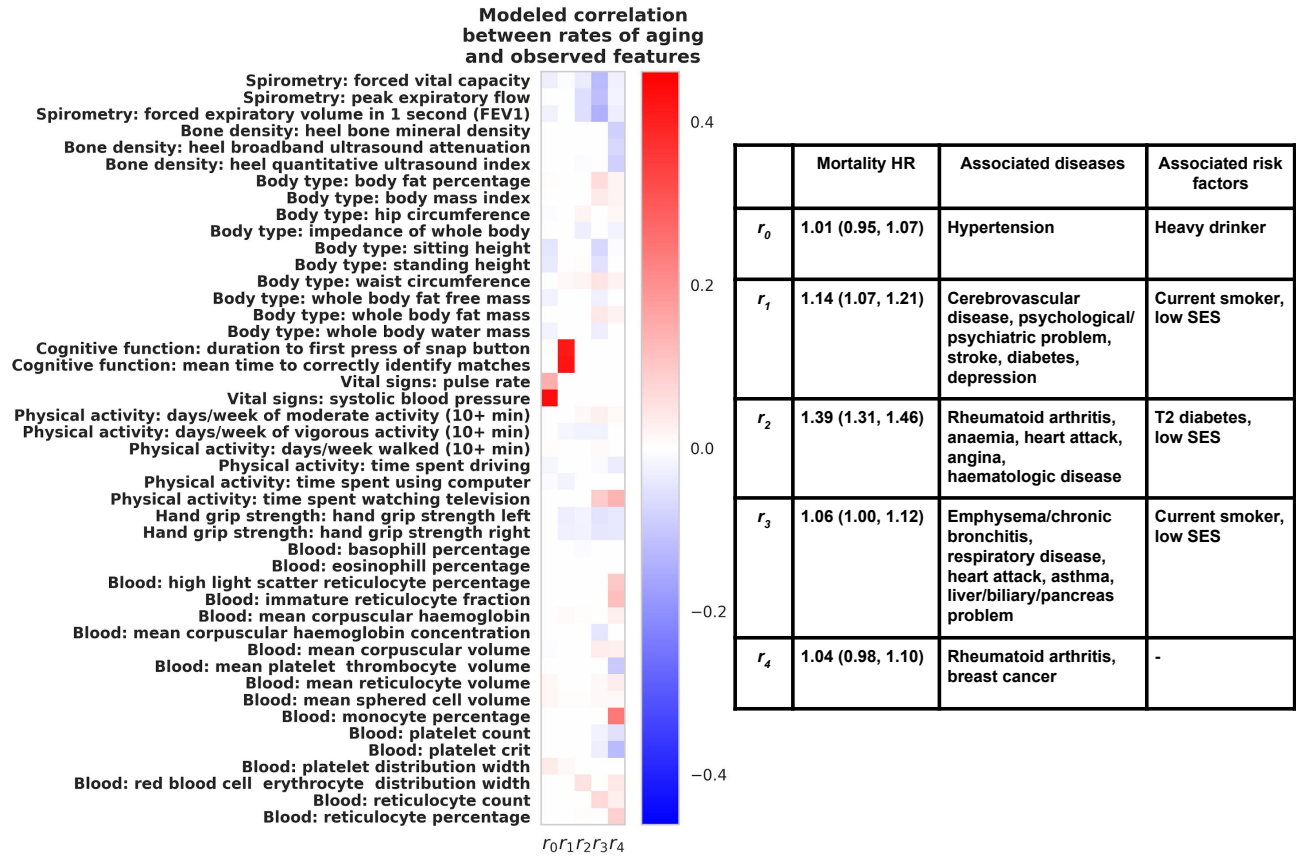


Figure 3. Left: model-learned correlations between rates of aging (columns) and observed features (rows) for monotonic features. Each cell displays the correlation between one rate of aging and one observed feature in data sampled from the model. Right: associations with mortality, diseases, and rate-of-aging risk factors. Mortality HR denotes the hazard ratio for a one-standard-deviation increase in rate of aging in a Cox proportional hazards model. The final two columns list the diseases and risk factors most strongly positively associated with higher rates of aging. We list up to five significant ( $p < 0.05$  after Bonferroni correction) and strong (effect size of a greater than 1% increase in the rate of aging) associations for each rate.

In addition, we examined associations between each rate of aging and three external sets of covariates not used in fitting the model: mortality; 91 diseases; and 5 risk factors which are known to accelerate aging processes, such as being a current smoker. We show these associations in Figure 3 (see Appendix B for details). Rates of aging were positively associated with all three sets of covariates: of the 88 statistically significant associations with diseases ( $p < 0.05$  after Bonferroni correction), 78% were positive; 73% of the 15 statistically associations with risk factors were positive, and all associations with mortality were positive although—interestingly—to widely varying degrees.

Based on these associations, we interpret the rates of aging as follows:  $r_0$ , a “blood pressure rate of aging”, associates with blood pressure and hypertension.  $r_1$ , a “cognitive rate of aging”, associates with our two cognitive function phenotypes. Consistent with this, it also associates with cognitive diseases (e.g., psychiatric problems, strokes, and depres-

sion).  $r_2$  is the most strongly associated with mortality, likely because of its associations with heart conditions including heart attacks and angina.  $r_3$ , a “lung rate of aging”, associates with pulmonary function and lung diseases (e.g., bronchitis and asthma), and is elevated in current smokers. Finally,  $r_4$ , a “blood and bone rate of aging”, correlates with blood phenotypes (e.g., monocyte percentage and platelet count) and with rheumatoid arthritis, an autoimmune disorder associated with changes in monocyte and platelet levels (Milovanovic et al., 2004; Rossol et al., 2012). Interestingly,  $r_4$  also correlates with all three bone density phenotypes, a direction for future study.

### 7.3. Learning from both cross-sectional and longitudinal data

Our model can naturally incorporate any available longitudinal data by optimizing the joint likelihood of the cross-sectional and longitudinal data. As cross-sectional and lon-

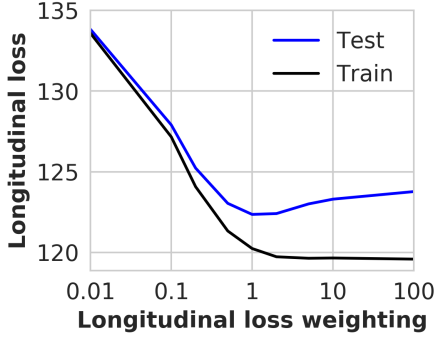


Figure 4. Longitudinal loss as a function of  $\lambda_{lon}$ .

gitudinal data can display different biases (Fry et al., 2017; Louis et al., 1986; Kraemer et al., 2000), this can produce models that are less affected by the biases in a particular dataset.

We handle longitudinal data similarly to cross-sectional data, but with an additional term in the model objective that captures the expected log-likelihood of observing the longitudinal follow-up  $x_{t_1}$  given our posterior of  $r$  and  $b$ . We control the relative weighting between cross-sectional and longitudinal data with a single parameter  $\lambda_{lon}$ ; when  $\lambda_{lon} = 1$ , the longitudinal and cross-sectional losses per sample are equally weighted; when  $\lambda_{lon} = 0$ , the model tries to fit only the cross-sectional data, and when  $\lambda_{lon} \gg 1$ , the model tries to fit only the longitudinal data. We fit the longitudinal model using the same model architecture and hyperparameters as the cross-sectional experiments above (Appendix C), varying only the longitudinal loss weighting  $\lambda_{lon}$ .

We search over a range of values of  $\lambda_{lon}$  and find that test longitudinal loss (i.e., the negative evidence lower bound on the likelihood of  $x_{t_0}$  and  $x_{t_1}$ ) is minimized when  $\lambda_{lon} = 1$ . This indicates that the model achieves the best longitudinal generalization performance by using cross-sectional data and the small amount of available longitudinal data (Figure 4, blue line). With higher  $\lambda_{lon}$ , the model overfits to the small longitudinal dataset. Repeating our longitudinal extrapolation task (Section 7.1) on a held-out test set of 1687 participants with longitudinal data, we found that the model with  $\lambda_{lon} = 1$  outperforms just predicting  $x_{t_0}$  on 83% of people with followups  $> 5$  years (compared to 66% with purely cross-sectional data, as in Section 7.1); pure reconstruction on 79% (vs 61%); and the average-cross-sectional-change baseline on 80% (vs. 60%). The longitudinal model also outperforms baselines on the full longitudinal dataset (as opposed to just individuals with followups  $> 5$  years) by similarly large margins. These results illustrate the benefits of methods which exploit both cross-sectional and longitudinal data.

## 8. Related work

**Biological age.** In our work, we interpreted the vector  $rt$  as the “biological age” of an individual. The notion of biological age as a measurable quantity that tracks chronological age on average, but captures an individual’s “true age”, dates back 50 years (Comfort, 1969). A common approach to quantifying it is to regress chronological age against a set of phenotypes and call the predicted quantity biological age (Furukawa et al., 1975; Borkan & Norris, 1980; Horvath, 2013; Chen et al., 2016; Putin et al., 2016); see also (Klemera & Doubal, 2006; Levine, 2012). These methods estimate a single-dimensional biological age and do not provide a way to make longitudinal inferences. Belsky et al. (2015) estimates a single-dimensional rate of aging, but requires longitudinal data.

**Pseudotime methods in molecular biology.** These methods order biological samples (for example, microarray data (Magwene et al., 2003; Gupta & Bar-Joseph, 2008) or RNA-seq data (Reid & Wernisch, 2016; Kumar et al., 2017)) using their gene expression levels; the imputed temporal order is referred to as *pseudotime*. Many of these methods assume that cells start out with the same observed expression levels and progress along the same single-dimensional trajectory at different rates; they construct trajectories by constructing a minimum spanning tree over the individual data points and minimizing the difference between points predicted as temporally adjacent (Qiu et al., 2011; Trapnell et al., 2014; Bendall et al., 2014). Gupta & Bar-Joseph (2008) showed recoverability of such methods under similar assumptions. Other methods use a Bayesian approach to estimate pseudotime (Campbell & Yau, 2017; Åijö et al., 2014). These methods all consider the case of a single-dimensional temporal trajectory (possibly with discrete branching points).

**Dimensionality reduction.** Others have studied aging on cross-sectional data using dimensionality reduction methods such as PCA (Nakamura et al., 1988) and factor analysis (MacDonald et al., 2004), using the first factor as the “aging dimension”. These dimensionality reduction methods do not explicitly take temporal information into account, and therefore do not cleanly factor out time-dependent changes from time-independent changes. Dimensionality reduction methods specific to time-series data, such as functional PCA, have been used to study clinically-relevant changes over time (Di et al., 2009; Greven et al., 2011) but require longitudinal data.

**Recovery of individual dynamics from cross-sectional data.** Recovering the behavior of individuals from population data has been studied in social science as ‘ecological inference’ (King, 2013). Learning dynamics from cross-sectional data has been studied under the label of ‘repeated



cross-section’ or ‘macro’ analysis (Moffitt, 1993; Collado, 1997; Kalbfleisch & Lawless, 1984; Plas, 1983; Hawkins & Han, 2000; Bernstein & Sheldon, 2016). These works focus on models without latent variables, and are restricted to linear or discrete time-series. Hashimoto et al. (2016) consider learning dynamics from cross-sectional data in more general settings, but still do not consider latent variable inference.

**Monotone function learning.** The task of learning partial monotone functions has been well-studied (Gupta et al., 2016; Daniels & Velikova, 2010; Qu & Hu, 2011; You et al., 2017). The main difficulty in applying these methods to our setting is that we require  $f^{-1}$  to be monotone (for identifiability) as well, which these methods do not guarantee; it is an open question if these methods can be adapted to learning order isomorphisms.

## 9. Discussion

We have presented a model that learns temporal dynamics from cross-sectional data. Each individual is represented by a low-dimensional latent state consisting of a dynamic vector  $rt$  which evolves linearly with time  $t$ , where  $r$  is an individual-specific rate vector, and a static vector  $b$  which captures age-independent variation. Constraining a subset of the observed features to be order-isomorphic in  $rt$  yields a model class in which rates of aging are identifiable. On real-world health data, our learned model is accurate and the rates of aging are interpretable.

Our proposed model is flexible, with many directions for future work. We could extend the model to incorporate more complexities of real-world data, including survivorship bias (Fry et al., 2017; Louis et al., 1986) or discontinuous changes in latent state (e.g, damage caused by a heart attack). Powerful previous ideas in latent variable models—for example, discrete latent variables (Jang et al., 2017; Maddison et al., 2016) that capture phenomena like sex differences, or placing hyperpriors on the model parameters—could be used to relax the parametric assumptions made by the model. Incorporating genetic information also represents a promising direction for future work. For example, genotype information could be used to learn rates of aging with a stronger genetic basis. We also anticipate that our learned rates of aging will be useful in downstream tasks like genome-wide association studies, where combining multiple phenotypes has been shown to increase power (O’Reilly et al., 2012). Finally, we hope that our model, by offering an identifiable, interpretable, and multi-dimensional characterization of temporal progression, can also be applied to longitudinal inference in domains other than human aging, like single-cell analysis.

**Acknowledgments** We would like to thank Zhenghao Chen, Jean Feng, Adam Freund, Noah Goodman, Mitchell Gordon, Steve Meadows, Baharan Mirzasoleiman, Chris Olah, Nat Roth, Camilo Ruiz, Christopher Yau, and the Calico UK Biobank team for helpful comments and discussion; EP was supported by Hertz and NDSEG Fellowships.

## References

- Äijö, T., Butty, V., Chen, Z., Salo, V., Tripathi, S., Burge, C. B., Lahesmaa, R., and Lähdesmäki, H. Methods for time series analysis of RNA-seq data with application to human Th17 cell differentiation. *Bioinformatics*, 30(12), 2014.
- Belsky, D. W., Caspi, A., Houts, R., Cohen, H. J., Corcoran, D. L., Danese, A., Harrington, H., Israel, S., Levine, M. E., Schaefer, J. D., et al. Quantification of biological aging in young adults. *Proceedings of the National Academy of Sciences*, 112(30), 2015.
- Bendall, S. C., Davis, K. L., Amir, E. D., Tadmor, M. D., Simonds, E. F., Chen, T. J., Shenfeld, D. K., Nolan, G. P., and Pe’er, D. Single-cell trajectory detection uncovers progression and regulatory coordination in human B cell development. *Cell*, 157(3):714–725, 2014.
- Bernstein, G. and Sheldon, D. Consistently estimating Markov chains with noisy aggregate data. In *Artificial Intelligence and Statistics (AISTATS)*, pp. 1142–1150, 2016.
- Borkan, G. A. and Norris, A. H. Assessment of biological age using a profile of physical parameters. *Journal of Gerontology*, 35(2):177–184, 1980.
- Campbell, K. and Yau, C. Uncovering genomic trajectories with heterogeneous genetic and environmental backgrounds across single-cells and populations. *bioRxiv*, 2017.
- Chen, B. H., Marioni, R. E., Colicino, E., Peters, M. J., Ward-Caviness, C. K., Tsai, P., Roetker, N. S., Just, A. C., Demerath, E. W., Guan, W., et al. DNA methylation-based measures of biological age: meta-analysis predicting time to death. *Aging (Albany NY)*, 8(9), 2016.
- Collado, M. D. Estimating dynamic models from time series of independent cross-sections. *Journal of Econometrics*, 82(1):37–62, 1997.
- Comfort, A. Test-battery to measure ageing-rate in man. *The Lancet*, 294(7635):1411–1415, 1969.
- Daniels, H. and Velikova, M. Monotone and partially monotone neural networks. *IEEE Transactions on Neural Networks*, 21(6):906–917, 2010.

- Di, C., Crainiceanu, C. M., Caffo, B. S., and Punjabi, N. M. Multilevel functional principal component analysis. *The Annals of Applied Statistics*, 3(1), 2009.
- EuYu. A non-negative matrix has a non-negative inverse. What other properties does it have? <https://math.stackexchange.com/q/214401>, 2012.
- Fry, A., Littlejohns, T. J., Sudlow, C., Doherty, N., Adamska, L., Sprosen, T., Collins, R., and Allen, N. E. Comparison of sociodemographic and health-related characteristics of UK Biobank participants with those of the general population. *American Journal of Epidemiology*, 186(9): 1026–1034, 2017.
- Furukawa, T., Inoue, M., Kajiya, F., Inada, H., Takasugi, S., Fukui, S., Takeda, H., and Abe, H. Assessment of biological age by multiple regression analysis. *Journal of Gerontology*, 30(4):422–434, 1975.
- Goodpaster, B. H., Park, S. W., Harris, T. B., Kritchevsky, S. B., Nevitt, M., Schwartz, A. V., Simonsick, E. M., Tylavsky, F. A., Visser, M., and Newman, A. B. The loss of skeletal muscle strength, mass, and quality in older adults: the health, aging and body composition study. *The Journals of Gerontology Series A: Biological Sciences and Medical Sciences*, 61(10):1059–1064, 2006.
- Greven, S., Crainiceanu, C., Caffo, B., and Reich, D. Longitudinal functional principal component analysis. *Recent Advances in Functional Data Analysis and Related Topics*, 2011.
- Gupta, A. and Bar-Joseph, Z. Extracting dynamics from static cancer expression data. *IEEE/ACM Transactions on Computational Biology and Bioinformatics (TCBB)*, 5(2):172–182, 2008.
- Gupta, M., Cotter, A., Pfeifer, J., Voevodski, K., Canini, K., Mangylov, A., Moczydlowski, W., and Esbroeck, A. V. Monotonic calibrated interpolated look-up tables. *Journal of Machine Learning Research (JMLR)*, 17(1): 3790–3836, 2016.
- Hashimoto, T., Gifford, D., and Jaakkola, T. Learning population-level diffusions with generative RNNs. In *International Conference on Machine Learning (ICML)*, pp. 2417–2426, 2016.
- Hawkins, D. and Han, C. Estimating transition probabilities from aggregate samples plus partial transition data. *Biometrics*, 56(3):848–854, 2000.
- Hoffmann, J. J., Nabbe, K. C., and van den Broek, N. M. Effect of age and gender on reference intervals of red blood cell distribution width (RDW) and mean red cell volume (MCV). *Clinical Chemistry and Laboratory Medicine (CCLM)*, 53(12), 2015.
- Horvath, S. DNA methylation age of human tissues and cell types. *Genome Biology*, 14(10), 2013.
- Jang, E., Gu, S., and Poole, B. Categorical reparameterization with Gumbel-softmax. *arXiv preprint arXiv:1611.01144*, 2017.
- Jonsen, I. D., Flemming, J. M., and Myers, R. A. Robust state-space modeling of animal movement data. *Ecology*, 86(11):2874–2880, 2005.
- Kalbfleisch, J. D. and Lawless, J. F. Least-squares estimation of transition probabilities from aggregate data. *Canadian Journal of Statistics*, 12(3):169–182, 1984.
- King, G. *A Solution to the Ecological Inference Problem: Reconstructing Individual Behavior from Aggregate Data*. Princeton University Press, 2013.
- Kingma, D. and Ba, J. Adam: A method for stochastic optimization. *arXiv preprint arXiv:1412.6980*, 2014.
- Kingma, D. P. and Welling, M. Auto-encoding variational Bayes. *arXiv*, 2014.
- Klemera, P. and Doubal, S. A new approach to the concept and computation of biological age. *Mechanisms of Ageing and Development*, 127(3):240–248, 2006.
- Kraemer, H. C., Yesavage, J. A., Taylor, J. L., and Kupfer, D. How can we learn about developmental processes from cross-sectional studies, or can we? *American Journal of Psychiatry*, 157(2):163–171, 2000.
- Kumar, P., Tan, Y., and Cahan, P. Understanding development and stem cells using single cell-based analyses of gene expression. *Development*, 144(1):17–32, 2017.
- Lane, J. M., Vlasac, I., Anderson, S. G., Kyle, S. D., Dixon, W. G., Bechtold, D. A., Gill, S., Little, M. A., Luik, A., Loudon, A., et al. Genome-wide association analysis identifies novel loci for chronotype in 100,420 individuals from the UK biobank. *Nature Communications*, 7, 2016.
- Levine, M. E. Modeling the rate of senescence: can estimated biological age predict mortality more accurately than chronological age? *Journals of Gerontology Series A: Biomedical Sciences and Medical Sciences*, 68(6): 667–674, 2012.
- Louis, T. A., Robins, J., Dockery, D. W., Spiro, A., and Ware, J. H. Explaining discrepancies between longitudinal and cross-sectional models. *Journal of Clinical Epidemiology*, 39(10):831–839, 1986.
- MacDonald, S. W., Dixon, R. A., Cohen, A., and Hazlitt, J. E. Biological age and 12-year cognitive change in older adults: findings from the victoria longitudinal study. *Gerontology*, 50(2):64–81, 2004.

- Maddison, C. J., Mnih, A., and Teh, Y. W. The concrete distribution: A continuous relaxation of discrete random variables. *arXiv preprint arXiv:1611.00712*, 2016.
- Magwene, P. M., Lizardi, P., and Kim, J. Reconstructing the temporal ordering of biological samples using microarray data. *Bioinformatics*, 19(7):842–850, 2003.
- McClearn, G. E. Biogerontologic theories. *Experimental Gerontology*, 32(1):3–10, 1997.
- Milovanovic, M., Nilsson, E., and Järemo, P. Relationships between platelets and inflammatory markers in rheumatoid arthritis. *Clinica Chimica Acta*, 343(1):237–240, 2004.
- Moffitt, R. Identification and estimation of dynamic models with a time series of repeated cross-sections. *Journal of Econometrics*, 59(1):99–123, 1993.
- Mozaffarian, D., Hao, T., Rimm, E. B., Willett, W. C., and Hu, F. B. Changes in diet and lifestyle and long-term weight gain in women and men. *New England Journal of Medicine*, 364(25):2392–2404, 2011.
- Nakamura, E., Miyao, K., and Ozeki, T. Assessment of biological age by principal component analysis. *Mechanisms of Ageing and Development*, 46(1):1–18, 1988.
- Nowell, P. C. The clonal evolution of tumor cell populations. *Science*, 194(4260):23–28, 1976.
- O’Reilly, P. F., Hoggart, C. J., Pomyen, Y., Calboli, F. C., Elliott, P., Jarvelin, M., and Coin, L. J. MultiPhen: joint model of multiple phenotypes can increase discovery in GWAS. *PloS One*, 7(5), 2012.
- Plas, A. P. V. D. On the estimation of the parameters of Markov probability models using macro data. *Annals of Statistics*, 1:78–85, 1983.
- Putin, E., Mamoshina, P., Aliper, A., Korzinkin, M., Moskalev, A., Kolosov, A., Ostrovskiy, A., Cantor, C., Vijg, J., and Zhavoronkov, A. Deep biomarkers of human aging: application of deep neural networks to biomarker development. *Aging*, 8(5), 2016.
- Qiu, P., Gentles, A. J., and Plevritis, S. K. Discovering biological progression underlying microarray samples. *PLoS Computational Biology*, 7(4), 2011.
- Qu, Y. and Hu, B. Generalized constraint neural network regression model subject to linear priors. *IEEE Transactions on Neural Networks*, 22(12):2447–2459, 2011.
- Ram, R. Government size and economic growth: A new framework and some evidence from cross-section and time-series data. *The American Economic Review*, 76(1): 191–203, 1986.
- Reid, J. E. and Wernisch, L. Pseudotime estimation: deconvolving single cell time series. *Bioinformatics*, 32(19): 2973–2980, 2016.
- Relethford, J. H., Lees, F. C., and Byard, P. J. The use of principal components in the analysis of cross-sectional growth data. *Human Biology*, pp. 461–475, 1978.
- Rossol, M., Kraus, S., Pierer, M., Baerwald, C., and Wagner, U. The CD14brightCD16+ monocyte subset is expanded in rheumatoid arthritis and promotes expansion of the Th17 cell population. *Arthritis & Rheumatology*, 64(3): 671–677, 2012.
- Stanojevic, S., Wade, A., Stocks, J., Hankinson, J., Coates, A. L., Pan, H., Rosenthal, M., Corey, M., Lebecque, P., and Cole, T. J. Reference ranges for spirometry across all ages: a new approach. *American Journal of Respiratory and Critical Care Medicine*, 177(3):253–260, 2008.
- Stein, E. M. and Shakarchi, R. *Fourier Analysis: an Introduction*, volume 1. Princeton University Press, 2011.
- Sudlow, C., Gallacher, J., Allen, N., Beral, V., Burton, P., Danesh, J., Downey, P., Elliott, P., Green, J., Landray, M., et al. UK Biobank: an open access resource for identifying the causes of a wide range of complex diseases of middle and old age. *PLoS Medicine*, 12(3), 2015.
- Trapnell, C., Cacchiarelli, D., Grimsby, J., Pokharel, P., Li, S., Morse, M., Lennon, N. J., Livak, K. J., Mikkelsen, T. S., and Rinn, J. L. The dynamics and regulators of cell fate decisions are revealed by pseudotemporal ordering of single cells. *Nature Biotechnology*, 32(4), 2014.
- Waddington, C. H. *Organisers and Genes*. University Press; Cambridge, 1940.
- Wain, L. V., Shrine, N., Miller, S., Jackson, V. E., Ntalla, I., Artigas, M. S., Billington, C. K., Kheirallah, A. K., Allen, R., Cook, J. P., et al. Novel insights into the genetics of smoking behaviour, lung function, and chronic obstructive pulmonary disease (UK Biobank): a genetic association study in UK Biobank. *The Lancet Respiratory Medicine*, 3(10):769–781, 2015.
- You, S., Ding, D., Canini, K., Pfeifer, J., and Gupta, M. Deep lattice networks and partial monotonic functions. In *Advances in Neural Information Processing Systems (NIPS)*, pp. 2985–2993, 2017.

## A. Proofs

### A.1. Non-negative and monomial matrices

In this section, we show that if the inverse of a non-negative matrix  $A$  exists and is itself non-negative, then  $A$  has to be a monomial matrix. This is a known linear algebra fact; we provide a proof for completeness, adapted from (EuYu, 2012).

**Definition 3.** A matrix  $A$  is called a non-negative matrix if all of its elements are  $\geq 0$ , and a positive matrix if all of its elements are  $> 0$ .

**Definition 4.** A matrix  $A$  is called a monomial matrix if it has exactly one non-zero entry in each row and each column. In other words, it has the same sparsity pattern as a permutation matrix, though the non-zero elements are allowed to differ from one.

**Lemma 3.** If  $A$  is an invertible non-negative matrix and  $A^{-1}$  is also non-negative, then  $A$  must be a non-negative monomial matrix.

*Proof.* Since  $A$  is invertible, every row of  $A$  must have at least one non-zero element. Consider the  $i$ -th row of  $A$ , and pick  $j$  such that  $A_{ij} \neq 0$ . Since  $AA^{-1} = I$ , we have that the dot product of the  $i$ -th row of  $A$  with the  $k$ -th column of  $A^{-1}$  must be 0 for all  $i \neq k$ . As  $A$  and  $A^{-1}$  are both non-negative, this dot product can only be 0 if every term in it is 0, including the product of  $A_{ij}$  with  $A_{jk}^{-1}$ . However,  $A_{ij} \neq 0$  by construction, so  $A_{jk}^{-1}$  must be 0 for all  $i \neq k$ . In other words, the  $j$ -row of  $A^{-1}$  must be all 0 except for  $A_{ji}^{-1}$ .

Applying a symmetric argument, we conclude that the  $i$ -th row of  $A$  must be all 0 except for  $A_{ij}$ . Since this holds for all  $i$ , we have that  $A$  must have exactly one non-zero in each row. Moreover, these non-zeros must appear in distinct columns, else  $A$  would be singular. We thus conclude that  $A$  must be a monomial matrix.  $\square$

### A.2. The Jacobians of monotone and order isomorphic functions

We recall the definition of monotone and order isomorphic functions from the main text:

**Definition 1.** A function  $f$  is monotone if  $u \preceq v \implies f(u) \preceq f(v)$  for all  $u, v \in \text{dom}(f)$ , where ordering is taken with respect to the positive orthant (i.e.,  $u \preceq v$  means  $u_i \leq v_i$  for all  $i$ ).

**Definition 2.** An injective function  $f$  is an order isomorphism if  $f$  and  $f^{-1}$  restricted to the image of  $f$  are both monotone, that is,  $u \preceq v \iff f(u) \preceq f(v)$ .

In this section, we establish that monotonicity and order isomorphism impose strong constraints on the function Jacobians.

**Lemma 4.** If a function  $f: \mathbb{R}^{k_r} \rightarrow \mathbb{R}^{k_r}$  is twice differentiable and monotone, then the Jacobian of  $f$  evaluated at any  $z \in \mathbb{R}^{k_r}$  is a non-negative matrix.

*Proof.* Assume for contradiction that  $f$  is differentiable and monotone, but that there exists some  $z \in \mathbb{R}^{k_r}$  such that the Jacobian  $J_f(z)$  is not a non-negative matrix. By definition, this implies that we can find  $i$  and  $j$  such that the  $ij$ -th entry of  $J_f(z)$  is negative.

Let  $e_j$  represent the  $j$ -th unit vector. By the remainder bound for Taylor approximations, twice differentiability implies that for any compact ball around  $z$ , we can find some constant  $M$  such that we can write  $f(z + \delta e_j) \leq f(z) + \delta J_f(z)e_j + \frac{M}{2}\delta^2$ . If we pick  $\delta < 2|J_f(z)_{ij}|/M$ , the first order term dominates. Since the  $ij$ -th entry is negative, this means that  $f_i(z + \delta e_j) < f_i(z)$  even though  $z + \delta e_j \succeq z$ , contradicting the monotonicity of  $f$ .  $\square$

**Lemma 5.** If  $q: \mathbb{R}^{k_r} \rightarrow \mathbb{R}^{k_r}$  is twice continuously differentiable and an order isomorphism, then the Jacobian matrix  $J_h(z)$  is a non-negative monomial matrix for all  $z \in \mathbb{R}^{k_r}$ .

*Proof.* If  $q$  is an order isomorphism, then  $q$  and  $q^{-1}$  are both monotone. By Lemma 4, their respective Jacobian matrices are non-negative everywhere.

Now, for any  $z \in \mathbb{R}^{k_r}$ , the inverse function theorem tells us that  $[J_q(z)]^{-1} = J_{q^{-1}}(q(z))$ , so both  $J_q(z)$  and its inverse  $[J_q(z)]^{-1}$  are non-negative. Applying Lemma 3 gives us that  $J_q(z)$  is a non-negative monomial matrix.  $\square$

### A.3. Component-wise monotonicity of order isomorphisms (Lemma 1 in main text)

The conditions on the Jacobian of a twice differentiable order isomorphic function  $q$  imply a constrained form.

**Lemma 1.** If  $q: \mathbb{R}^{k_r} \rightarrow \mathbb{R}^{k_r}$  is an order isomorphism and twice continuously differentiable,  $q$  must be expressible as a permutation followed by a component-wise strictly monotone transform.

*Proof.* Since  $q$  is bijective,  $q^{-1}$  exists everywhere, which implies that  $J_q(r)$  must have full rank everywhere. Since  $J_q(r)$  is a monomial matrix by Lemma 5, this means that the sparsity pattern of  $J_q(r)$  cannot vary with  $r$ ; otherwise, by the intermediate value theorem, there will be some  $r$  where  $J_q(r)$  where a row has greater than one nonzero or no nonzeros and thus is not monomial. By definition, a monomial matrix can be decomposed into a positive diagonal matrix and a permutation. Applying the fundamental theorem of calculus to each diagonal entry recovers the strictly monotone transform, and the permutation matrix defines the permutation. The existence of the antiderivative is guaranteed by construction of  $J_q$  as the derivative of  $q$ .  $\square$

#### A.4. Identifiability in the noiseless setting (Proposition 1 in main text)

We start by establishing two helpful lemmas:

**Lemma 6.** *If functions  $f_1$  and  $f_2$  are both monotone, then  $f_1 \circ f_2$  is also monotone.*

*If  $f_1$  and  $f_2$  are both bijective order isomorphisms, then  $q \stackrel{\text{def}}{=} f_2^{-1} \circ f_1$  is also a bijective order isomorphism.*

*Proof.* The first part of the lemma follows from the transitivity of partial orders:  $x \prec y \implies f_1(x) \prec f_1(y) \implies f_2(f_1(x)) \prec f_2(f_1(y))$ .

For the second part, note that  $q$  is bijective because it is the composition of two bijective functions. Now, since  $f_1$  and  $f_2$  are both order isomorphisms, we know that  $f_1, f_1^{-1}, f_2$ , and  $f_2^{-1}$  are all monotone. By the first part of the lemma, we conclude that  $q = f_2^{-1} \circ f_1$  and  $q^{-1} = f_1^{-1} \circ f_2$  are both monotone, implying that  $q$  is an order isomorphism.  $\square$

**Lemma 7.** *If a continuous, univariate, strictly monotone function  $q_i$  is measure preserving for a random variable  $x$ ,  $q_i$  must be the identity map (on the support of  $x$ ).*

*Proof.* By strict monotonicity,  $c_1 < c_2$  implies  $q(c_1) < q(c_2)$  and thus the CDF is preserved implying that  $P(x < c) = P(q(x) < q(c)) = P(x < q(c))$ . The last step follows from measure preservation of  $q$ .

Now assume for contradiction that  $q_i$  is not the identity map. We can then pick some  $c$  such that  $q(c) \neq c$  and  $P(c) > 0$ . This implies that  $P(x < q(c)) \neq P(x < c)$  which is a contradiction.  $\square$

We can now state and prove identifiability in the noiseless setting:

**Proposition 1.** *If  $f_1$  and  $f_2$  and their inverses are twice continuously differentiable and order-isomorphic functions such that  $f_1(tr) \stackrel{(d)}{=} f_2(tr) \stackrel{(d)}{=} x_t$  for some  $t > 0$ , then  $f_1$  and  $f_2$  are identical up to a permutation.*

*Proof.* We consider the difference map  $q \stackrel{\text{def}}{=} f_2^{-1} \circ f_1$ , which maps latent rates of aging implied by  $f_1$  to that of  $f_2$ . Our aim is to show that  $q$  must be a permutation, which will give the desired result.

From Lemma 6, we know that  $q$  is itself an order isomorphism. Thus, by Lemma 1, it must be expressible as the composition of a component-wise strictly monotone map and a permutation.

We can further show that this component-wise strictly monotone transformation has to be the identity transformation. Since both  $f_1$  and  $f_2$  map  $rt \mapsto x_t$ ,  $q$  is measure preserving on  $rt$ . In other words, it maps the probability distribution of

$rt$  to itself. We can therefore apply Lemma 7 to conclude that  $q$  can only be a permutation.

Applying  $f_2$  to both sides of  $q = f_2^{-1} \circ f_1$ , we get that  $f_1$  and  $f_2$  have to be permutations of each other, as desired.  $\square$

#### A.5. Checking order isomorphisms (Lemma 2 and Proposition 2 in main text)

**Lemma 2.** *Let  $a(x) = Ax$ , where  $A \in \mathbb{R}^{d \times k}$ . If we can write  $A = P \begin{bmatrix} B \\ C \end{bmatrix}$  where  $P$  is a permutation matrix,  $B$  is a non-negative monomial matrix, and  $C$  is a non-negative matrix, then  $a$  is an order isomorphism.*

*Proof.*  $a$  is monotone since  $A$  is non-negative. To verify that the inverse of  $a$  over its image is monotone, let  $I_k = [I; 0] \in \mathbb{R}^{k \times d}$  be the matrix selecting the first  $k$  coordinates. If  $Ax \prec Ay$ , every coordinate of  $Ax$  is smaller than the corresponding coordinate of  $Ay$ , so we can jointly permute the rows (i.e., left-multiplying by a permutation matrix) or select a subset of coordinates while preserving ordering. Thus,  $Ax \prec Ay \implies I_k P^{-1} Ax \prec I_k P^{-1} Ay$ . By construction,  $I_k P^{-1} A = B$  is a non-negative monomial matrix. Applying a similar permutation argument, we have that  $I_k P^{-1} Ax \prec I_k P^{-1} Ay \implies x \prec y$ .  $\square$

**Proposition 2.** *Let  $f: \mathbb{R}^k \rightarrow \mathbb{R}^d = s_2 \circ a \circ s_1$ , where  $s_1: \mathbb{R}^k \rightarrow \mathbb{R}^k$  and  $s_2: \mathbb{R}^d \rightarrow \mathbb{R}^d$  are continuous, component-wise monotone transformations, and  $a: \mathbb{R}^k \rightarrow \mathbb{R}^d$  is a linear transform. If  $a$  satisfies Lemma 2, then  $f$  is an order isomorphism.*

*Proof.* The proof follows from the fact that order preservation is transitive.  $a \circ s_1$  is an order isomorphism onto its image, since  $s_1$  is an order isomorphism on the entire  $\mathbb{R}^k$  and  $a$  is order isomorphic onto its image by Lemma 2. Thus for any  $x \prec y \iff a(s_1(x)) \prec a(s_1(y))$ . Since  $s_2$  is an order isomorphism on  $\mathbb{R}^d$ , we have  $x \prec y \iff a(s_1(x)) \prec a(s_1(y)) \iff s_2(a(s_1(x))) \prec s_2(a(s_1(y)))$ .  $\square$

## B. UK Biobank dataset and processing

**Phenotype filtering.** We selected Biobank phenotypes that were measured for a large proportion of the dataset and that captured diverse and important dimensions of aging and general health. After removing phenotypes which were missing data for many people, redundant (e.g., there are multiple measurements of BMI), or discrete (e.g., categorical responses from a survey question), we were left with 52 phenotypes (Table 1). By visual inspection, we categorized the 52 phenotypes into monotone features (45/52) and non-monotone features (7/52) for the cross-sectional model. In the combined longitudinal/cross-sectional model,

we modeled an additional 8 features as non-monotone because they increased in the longitudinal data but not in the cross-sectional data, or vice versa.

**Sample filtering.** We removed individuals with non-European ancestry, as identified from their genetic principal components, as is commonly done in studies of the UK Biobank to minimize spurious correlations with ancestry particularly in genetic analysis (Lane et al., 2016; Wain et al., 2015). (The vast majority of individuals in UK Biobank are of European ancestry.) We also removed individuals who were missing data in any of our selected phenotypes.

After filtering, we were left with a train/development set of 213,510 individuals; we report all results on a test set of 53,174 individuals not used in model development or selection. While these samples are cross-sectional (with a measurement at only a single timepoint), we have a single longitudinal followup visit for an additional 8,470 individuals, on which we assess longitudinal progression. UK Biobank data contains two followup visits; we use only longitudinal data from the first followup visit (2-6 years after the initial visit), not the second, because some of the phenotypes we use in model fitting were not measured at the second followup.

**Phenotype processing.** We normalized each phenotype to have mean 0 and variance 1. In fitting the model, we first transformed all phenotypes so they were positively correlated with age, by multiplying all phenotypes which were not by negative one, so we could assume that monotone features were monotone increasing. However, all results in the paper are shown with the original phenotype signs.

**Diseases, mortality, and risk factors.** We examined associations with 91 diseases which were reported by at least 5,000 individuals in the entire UKBB dataset. Diseases were retrospectively assessed via interview (i.e., subjects developed the disease prior to the measurement of  $x_{t_0}$ ). Second, we examined associations between rates of aging and mortality. In contrast to disease status, mortality was measured after  $x_{t_0}$  (all subjects were obviously alive when  $x_{t_0}$  was measured); thus, examining associations with mortality serves as an indication that rates of aging predict future outcomes. Finally, we examined 5 binary risk factors: whether the individual currently smokes, if they are a heavy drinker, if they are above the 90th percentile in Townsend deprivation index (a measure of low socioeconomic status), if they have type 2 diabetes, and if they report no days of moderate or vigorous exercise in a typical week.

We examined associations between rates of aging and mortality using a Cox proportional hazards model which controlled for age, sex, and the first five genetic principal components. We report the hazard ratios for a one standard-

deviation increase in rate of aging. For the 5 binary risk factors and the 91 diseases, we examined associations using a linear regression model, where the dependent variable was the rate of aging and the independent variable was the risk factor or disease. We controlled for age, sex, and the first five genetic principal components. We filtered for associations which passed a statistical significance threshold of  $p = 0.05$ , with Bonferroni correction for the number of tests performed. Figure 3 reports the diseases/risk factors with the largest positive associations and an effect size of a greater than 1% increase in the rate of aging; if more than five diseases or risk factors pass this threshold, we report the top five.

## C. Model architecture and hyperparameters

**Hyperparameter selection.** We conducted a random search over the encoder architecture, decoder architecture, learning rate, elementwise nonlinearity, and whether there was an elementwise nonlinearity prior to the linear transformation matrix. We selected a configuration which performed well (as measured by low reconstruction error/high out-of-sample evidence lower bound (ELBO)) across a range of latent state sizes. Our final architecture uses a learning rate of 0.0005, encoder layer sizes of [50, 20] prior to the latent state, and decoder layer sizes of [20, 50]. Our elementwise nonlinearity is parameterized by  $s(y) = \sum_{p_i \in S} w_i y^{p_i}$ , where  $S = [\frac{1}{5}, \frac{1}{4}, \frac{1}{3}, \frac{1}{2}, 1, 2, 3, 4, 5]$ . We found that using an elementwise nonlinearity prior to the linear transformation was not necessary in our dataset, so we only used a nonlinearity after the linearity transformation for interpretability and ease in training. We used Adam for optimization (Kingma & Ba, 2014) and ReLUs as the nonlinearity.

**Combined longitudinal/cross-sectional model.** The loss for cross-sectional samples is the negative evidence lower bound (ELBO), as before. The loss for longitudinal samples has an additional term that captures the expected log-likelihood of observing the longitudinal follow-up  $x_{t_1}$  given our posterior of  $r$  and  $b$ . We use the same model architecture as for the cross-sectional model. In particular, to avoid overfitting on the small number of longitudinal samples, we share the same encoder; this means that the approximate posterior over  $r$  and  $b$  for a longitudinal sample is calculated only using  $x_{t_0}$ . Because we have far more cross-sectional samples than longitudinal samples, we train the model by sampling longitudinal batches with replacement, with one longitudinal batch for every cross-sectional batch. In addition to the 7 non-monotonic features used in the cross-sectional experiments, we add an additional 8 features to the non-monotonic list because they increase in longitudinal data and not in cross-sectional data, or vice versa (Table 1).



## Inferring Rates of Aging from Cross-Sectional Data

Table 1. UK Biobank features used in model fitting. \* denotes features which are modeled as non-monotone in age when fitting the cross-sectional model. \*\* denotes additional features which are modeled as non-monotone in age when fitting the model which uses both longitudinal and cross-sectional data. All features which are modeled as non-monotone in the cross-sectional analysis are also modeled as non-monotone in the combined longitudinal/cross-sectional model.

Feature
Spirometry: forced vital capacity
Spirometry: peak expiratory flow
Spirometry: forced expiratory volume in 1 second (FEV1)
Bone density: heel bone mineral density
Bone density: heel broadband ultrasound attenuation
Bone density: heel quantitative ultrasound index
Body type: body fat percentage
Body type: body mass index
Body type: hip circumference
Body type: impedance of whole body**
Body type: sitting height
Body type: standing height
Body type: waist circumference
Body type: whole body fat free mass
Body type: whole body fat mass
Body type: whole body water mass
Cognitive function: duration to first press of snap button
Cognitive function: mean time to correctly identify matches
Vital signs: diastolic blood pressure*
Vital signs: pulse rate**
Vital signs: systolic blood pressure
Physical activity: days/week of moderate activity (10+ min)
Physical activity: days/week of vigorous activity (10+ min)
Physical activity: days/week walked (10+ min)
Physical activity: time spent driving
Physical activity: time spent using computer**
Physical activity: time spent watching television
Hand grip strength: hand grip strength left
Hand grip strength: hand grip strength right
Blood: basophill percentage
Blood: eosinophill percentage
Blood: haematocrit percentage*
Blood: haemoglobin concentration*
Blood: high light scatter reticulocyte percentage
Blood: immature reticulocyte fraction
Blood: lymphocyte percentage*
Blood: mean corpuscular haemoglobin
Blood: mean corpuscular haemoglobin concentration**
Blood: mean corpuscular volume**
Blood: mean platelet thrombocyte volume
Blood: mean reticulocyte volume
Blood: mean sphered cell volume
Blood: monocyte percentage**
Blood: neutrophill percentage*
Blood: platelet count
Blood: platelet crit
Blood: platelet distribution width
Blood: red blood cell erythrocyte count*
Blood: red blood cell erythrocyte distribution width
Blood: reticulocyte count**
Blood: reticulocyte percentage**
Blood: white blood cell leukocyte count*